

Interactive Feature Embedding for Infrared and Visible Image Fusion

Fan Zhao, Wenda Zhao, Huchuan Lu

Abstract—General deep learning-based methods for infrared and visible image fusion rely on the unsupervised mechanism for vital information retention by utilizing elaborately designed loss functions. However, the unsupervised mechanism depends on a well designed loss function, which cannot guarantee that all vital information of source images is sufficiently extracted. In this work, we propose a novel interactive feature embedding in self-supervised learning framework for infrared and visible image fusion, attempting to overcome the issue of vital information degradation. With the help of self-supervised learning framework, hierarchical representations of source images can be efficiently extracted. In particular, interactive feature embedding models are tactfully designed to build a bridge between the self-supervised learning and infrared and visible image fusion learning, achieving vital information retention. Qualitative and quantitative evaluations exhibit that the proposed method performs favorably against state-of-the-art methods.

Index Terms—Infrared and visible image fusion, hierarchical representations, interactive feature embedding, self-supervised learning.

I. INTRODUCTION

VISIBLE image, captured by the reflected light of a scenario, contains abundant texture details. Complementarily, infrared image exhibits strong anti-interference ability (e.g., smoke and night) by capturing the thermal radiation. However, the detailed structure information is insufficiently in infrared image. Infrared and visible image fusion aims to construct a high-quality image by integrating the vital information from source images, which is more conducive to subsequent applications, such as security, monitoring, target tracking, and object recognition [1]–[4].

Vital feature extraction and fusion are keys associated with infrared and visible image fusion. On the one hand, visible image mainly represents the reflected light information with detailed textures, while infrared image depicts the thermal radiation information with high contrast pixel intensities (as shown in Fig. 1(a-b)). These two types of features have domain discrepancy, which needs special attention. On the other hand, both visible and thermal images contain some common vital features, such as brightness and object semantics. Thus, how to comprehensively extract and fuse aforementioned features, including universal features and domain discrepancy features, remains the major stumbling block.

To alleviate the above problems, previous methods can be mainly divided into three categories. (1) Hand-crafted feature-based methods implement image transform (e.g., multi-scale transform (MST) [5]–[7] and hybrid models [8]–[10]) to extract some specific information, such as contrast and textures. (2) Convolutional neural network (CNN)-based methods (e.g., DenseFuse [11], IFCNN [12] and U2Fusion [13]) learn to extract multi-level features, thereby fusing vital and domain discrepancy information. (3) Adversarial learning-based methods [14]–[16] intend to fuse thermal radiation information and textural detail information through adversarial training along with designed loss.

Although infrared and visible image fusion has made progress, previous methods generally have the following limitations. On the one hand, the same image transform or convolution operator can hardly extract comprehensive features. On the other hand, single-stage feature fusion may not make the fused image retain all vital features of source images. As shown in Fig. 1, the intensity information in visible image (e.g., the pavilion) and the texture information in infrared image (e.g., the man) are lost in Fig. 1(c), the intensity information of source images is not well preserved in Fig. 1(d) and Fig. 1(e), and low-contrast dilemmas exist in Fig. 1(f-g). Addressing the above problems, we propose self-supervised hierarchical feature extraction and stage-interactive feature fusion framework (IFESNet) for infrared and visible image fusion.

Specifically, we first conceive the self-supervised strategy for jointly source image reconstruction and fusion. As an auxiliary task, image reconstruction task is trained by regarding the source image as ground truth in a self-supervised way. Therefore, richer and more comprehensive features of source images can be learned. Compared with unsupervised mechanism, our self-supervised strategy can capture more informative representations. Furthermore, we propose an interactive feature embedding model (IFEM) to build a bridge between the self-supervised learning and infrared and visible image fusion learning, achieving vital information retention. IFEM is formulated by interacting hierarchical representations between fusion and reconstruction tasks. Specifically, the interaction process is recursively conducted in the corresponding hierarchical layers between reconstruction and fusion tasks. Note that the hierarchical representation interaction process is bi-directional. Therefore, we utilize the internal relationship between different tasks to efficiently extract and fuse these feature representations, improving the performance of fusion task.

As illustrated in Fig. 1(h), our IFESNet can retain larger amount of thermal radiation information (e.g., person) from

Fan Zhao is with School of Physics and Electronic Technology, Liaoning Normal University, Dalian, 116029, P.R. China. E-mail: Fan_Zhao20@163.com.

Wenda Zhao and Huchuan Lu are with the Key Laboratory of Intelligent Control and Optimization for Industrial Equipment of Ministry of Education and School of Information and Communication Engineering, Dalian University of Technology, Dalian, 116024, P.R. China. E-mail: zhaowenda@dlut.edu.cn, lhchuan@dlut.edu.cn.

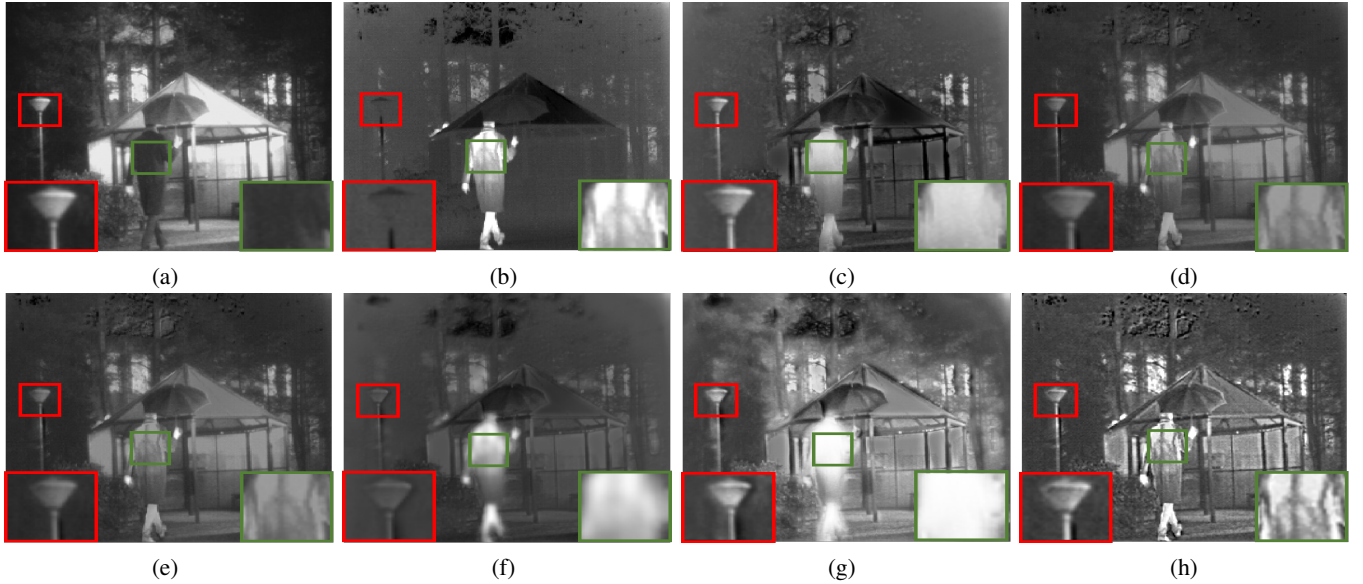


Fig. 1. Vital feature retention in fused images of different methods. (a-h) are visible image, infrared image, GTF, DeepFuse, DenseFuse, FusionGAN, DDCGAN and our IFESNet.

Fig. 1(b) and textural detail information (e.g., pavilions and trees) from Fig. 1(a). In addition, as shown in the locally enlarged areas, our fusion result can also effectively preserve the texture and edge information of Fig. 1(b) (e.g., the dorsal area of the person in green box), and high-contrast intensity information of Fig. 1(a) (e.g., street lamp in red box). On the contrary, GTF, FusionGAN and DDCGAN lose partial texture details in infrared image, while DeepFuse and DenseFuse lose some contrast information in visible image. Concretely, our contributions are:

- We make the first attempt to develop self-supervised strategy to solve the vital information missing dilemmas in infrared and visible image fusion. In contrast with the most widely used non-adversarial and adversarial fusion methods, our framework is simple yet effective, better improving the performance of fused image.
- Interactive feature embedding model is designed across fusion and reconstruction tasks, gradually extracting vital information representations and promoting fusion task.
- Compared with the state of the arts, our proposal can retain more vital features, including universal features and domain discrepancy features.

The remainder of the paper is organized as follows. Section II introduces the related work. Section III presents our proposed framework. In Section IV, qualitatively and quantitatively results are evaluated and analyzed, and ablation studies are conducted. Finally, Section V concludes this paper.

II. RELATED WORK

A. Hand-crafted Feature-based Methods

Varied attempts based on hand-crafted feature extraction have been proposed. For instance, multi-scale transform [5]–[7], sparse representation (SR) [17]–[21], subspace [22]–[24], hybrid models [8]–[10] and gradient [25] are widely

used. For improving feature extraction ability, Laplace pyramid [5], contourlet [6], gradient [26], SR [21], independent component analysis (ICA) [23], principal component analysis (PCA) [22], and nonnegative matrix factorization (NMF) [24]-based methods are developed, attempting to transform the source images with the same operation. As illustrated in Fig. 1, visible image mainly represents the reflected light information, while infrared image depicts the thermal radiation information. Inherently, these two types of features are specific to source image with domain discrepancy, which can hardly be represented in the same manner. In addition, hand-crafted features can not comprehensively represent all features of source images, resulting in limited performance.

B. Non-adversarial Fusion Methods

Deep learning models [11], [13], [27]–[35] for image fusion have been put forward, whereas feature extraction and fusion still remain an active topic. Liu *et al.* [29] firstly utilize a siamese convolutional network for weight map generation. To avoid the loss of vital features, similarity-based fusion strategy is adopted to adjust the decomposed coefficients. Li *et al.* [30] decompose infrared and visible images into base layers and detail content layers, and then use CNN for feature extraction of detail content layers. To boost feature extraction performance, DenseFuse [11] adopts dense block to construct feature maps. Xu *et al.* [13] propose U2Fusion, where the similarity between fusion result and source images is constraint for improving the vital information retention in an unsupervised way. For further enhancing the texture and intensity information, Zhang *et al.* [32] develop proportional maintenance of gradient and intensity (PMGI) network, in which path-wise transfer block is designed to avoid the vital information loss.

Those fusion frameworks, in spirit, can be roughly summarized as Fig. 2(b). As a whole, they focus on extracting and

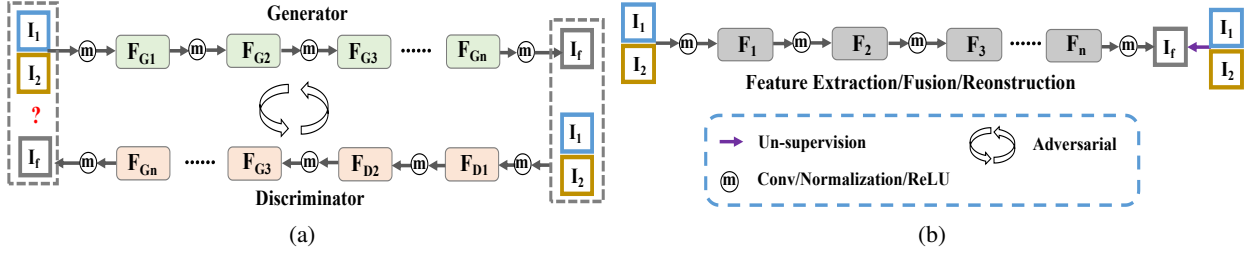


Fig. 2. Pipeline of varied types of fusion methods. (a-b) correspond to the adversarial fusion framework and non-adversarial fusion framework. The colorful box (F_G , F_D and F_n) represent hierarchical features. The arrows between blocks indicate the feature stream. I_1 , I_2 are source images. I_{r1} , I_{r2} are reconstructed results of source images, and I_f represents the final fusion result.

fusing vital features via unsupervised strategy, while loss function is designed to constrain the fusion results to contain the desired features. However, as illustrated in Fig. 1, it can hardly design a comprehensive and adaptive loss function covering all vital features. In other words, unsupervised mechanism is not capable enough to extract and fuse all vital features of source images.

C. Adversarial Fusion Methods

Adversarial fusion methods aim to formulate the fusion task as an adversarial learning, in which the thermal radiation information is fused while the visible texture information is retained. Ma *et al.* [14] develop FusionGAN, which generates the fusion results with infrared intensities and dominant visible gradients. On this basis, DDcGAN [15] adopts a generator with two discriminators to enhance the edge information of thermal targets with the specially designed content loss. Later, Ma *et al.* [16] design a variant based on detail preserving adversarial learning, where detail loss and target edge-enhancement loss are designed based on FusionGAN. This approach can greatly retain the vital features of source images compared with FusionGAN.

The overview of adversarial fusion methods can be roughly summarized as Fig. 2(a). A generator is adopted to produce a fused image I_f with major features of source images, and then a discriminator is used to distinguish I_f from source images. Hence, fusion task is achieved by this adversarial learning mechanism. However, adversarial process is difficult to optimize, which easily leads to distorted results. In addition, the feature diversity of source images, not only thermal radiation and gradient variation, but also the other common features, brings great difficulty for comprehensively covering all vital features. Consequently, any features (e.g., textures in infrared image or intensities in visible image) ignored by the loss function, will not be retained in the fusion results (as shown in Fig. 1(f-g)). Similarly, this can also be attributed to the limitation of unsupervised mechanism.

III. PROPOSED METHOD

A. Motivation

We are committed to alleviate vital feature loss dilemma. Infrared image and visible image are characterized by thermal radiation and visible gradient information, respectively. Their domain discrepancy needs special attention. On the

other hand, they contain common attribute features, such as gradient variation, intensity, contrast and saturability. Majority fusion methods adopt the same operator for feature extraction, resulting in limited performance for dealing with domain discrepancy features. Most importantly, existing fusion methods involve unsupervised strategy with elaborate loss functions for vital feature fusion. Such mechanism is not adequately for retaining all vital information. Since it is infeasible to design a comprehensive and adaptive loss function that covers all vital features. Ignoring any information (e.g., texture in infrared or intensity in visible) will result in vital feature missing (as shown in Fig. 1).

In this section, we develop a novel interactive feature embedding in self-supervised learning network (IFESNet) for infrared and visible image fusion. Different from the widely used unsupervised mechanism, we attempt to develop self-supervised strategy in cooperation with stage-interactive feature embedding learning to solve the issue of vital information missing. The pipeline is illustrated in Fig. 3. Several concepts have been considered to conceive such architecture, including 1) self-supervised hierarchical feature extraction for jointly reconstruction and fusion tasks in Section III.B, and 2) stage-interactive feature embedding learning in Section III.C. Please note that since pooling operation will reduce spatial resolution of features, our IFESNet consists of convolution layers to retain spatial details of the fused image effectively.

B. Self-supervised Hierarchical Feature Extraction

By self-supervised mechanism, we aim to achieve hierarchical feature extraction containing more informative representations, thereby boosting fusion performance. As shown in Fig. 3, IFESNet includes SHFENet-ir (self-supervised hierarchical feature extraction network of infrared image), SHFENet-vis (self-supervised hierarchical feature extraction network of visible image), and IVIFNet (infrared and visible image fusion network). In the following section, we will detail the self-supervised strategy for jointly reconstruction and fusion tasks.

Self-supervised Feature Extraction. Vital feature extraction is the premise of boosting fusion performance. Thus, we aim to extract hierarchical features F'_n and F''_n , which contain comprehensive features of infrared image I_1 and visible image I_2 . Essentially, this is achieved through reconstructing images I_{r1} and I_{r2} using the source image as ground truth in a self-supervised way. Since hierarchical features F'_n, F''_n can be

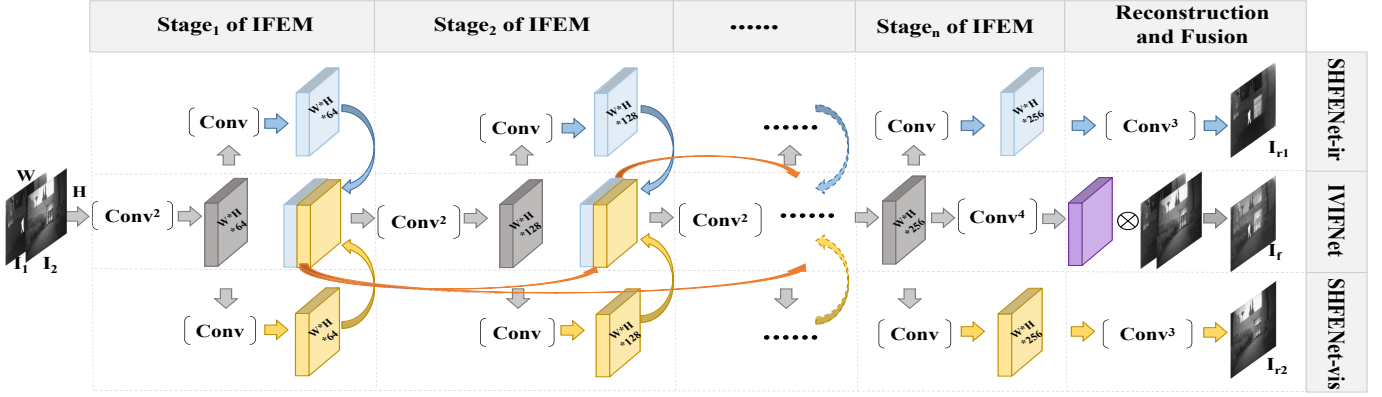


Fig. 3. The detailed architecture of interactive feature embedding in self-supervised learning network (IFESNet). In the horizontal direction, IFESNet is consisted by self-supervised hierarchical feature extraction network of infrared image (SHFENet-ir), self-supervised hierarchical feature extraction network of visible image (SHFENet-vis), and infrared and visible image fusion network (IVIFNet), where self-supervised hierarchical features are used for jointly reconstruction and fusion. In the vertical direction, IFESNet is consisted by multi stages of interactive feature embedding models (IFEM), which conducts hierarchical feature interaction stage-interactive between IVIFNet and SHFENet to gradually fuse vital information, thereby avoiding vital feature loss in fusion result. \otimes indicates channel-wise multiplication. $Conv^n$ denotes n times convolution operations. Note that only convolution layers are used for feature extraction.

reconstructed back to source images, it in turn ensures that the corresponding hierarchical layers are competent to extract vital features of source images.

Take the SHFENet-ir as an example (see Fig. 3). From the perspective of information flow, the SHFENet-ir is constructed by hierarchical feature interaction process between each layer of SHFENet-ir and IVIFNet. In particular, the hierarchical features F'_n and F''_n are totally obtained from the hierarchical feature F_n of IVIFNet, which can be formulated as

$$F'_n, F''_n = C(\underbrace{C^2(Cat(F'_{n-1}, F''_{n-1}))}_{F_n}), \quad (1)$$

where F'_n and F''_n denote the hierarchical features of layer n in SHFENet-ir and SHFENet-vis, respectively. F_n is hierarchical feature of IVIFNet. C and C^2 represent conducting convolution operation one and twice, respectively. Cat denotes the concatenation operation. For the last layer of SHFENet, the outputs are the reconstructed results, which can be formulated as

$$I_{r1} = C^3(F'_n), I_{r2} = C^3(F''_n), \quad (2)$$

where I_{r1} and I_{r2} denote reconstructed results of infrared and visible images, respectively. C^3 represents conducting convolution operation three times.

The self-supervised strategy ensures that hierarchical features F'_n, F''_n contain the main features of source image I_1, I_2 during reconstruction task. It is worth to note that the hierarchical features F'_n, F''_n of reconstruction task are totally obtained from the corresponding hierarchical features F_n of fusion task. Thus, F'_n, F''_n in turn constrain the hierarchical feature F_n of IVIFNet to possess the main features of I_1, I_2 . In other words, the self-supervised strategy promotes the fusion task. Specifically, SHFENet is constructed by six convolution layers with 3×3 kernels and 64, 128, 256, 128, 64 and 1 channels respectively. Note that down-sampling and up-sampling structures are not adopted in SHFENet, which can avoid the loss of effective information.

Hierarchical Feature Fusion. In IVIFNet, we aim to generate the fusion result utilizing hierarchical features obtained by self-supervised mechanism. Considering the extracted hierarchical features F'_n, F''_n cover sufficient information of source images, it is potential for encouraging fusion task. Thus, how to utilize these vital features for fusion task remains a problem to be solved.

To achieve this, the hierarchical feature interaction process between reconstruction and fusion task is designed to gradually promote the fusion network. As shown in Fig. 3, we first concatenate the source images I_1 and I_2 , and then the hierarchical feature F_1 can be obtained by conducting convolution operation $Conv$ twice. Based on the idea of merging and then separating features [36], we fuse the layer-wise hierarchical features F'_{n-1} and F''_{n-1} from SHFENet, and the hierarchical feature F_n of IVIFNet can be formulated as

$$F_n = C^2(Cat(\underbrace{C(F_{n-1})}_{F'_{n-1}}, \underbrace{C(F_{n-1})}_{F''_{n-1}})). \quad (3)$$

At this point, the hierarchical feature F_n of IVIFNet is derived from hierarchical features F'_{n-1}, F''_{n-1} , which heuristically shares low-, mid- and high-level features for fusion. Thus, the extracted hierarchical features F'_n, F''_n via self-supervised strategy can be fully utilized for fusion task, which in turn avoids the vital features missing in fusion result. Specifically, IVIFNet is constructed by ten convolution layers with 3×3 kernels and 64, 64, 128, 128, 256, 256, 256, 128, 64 and 1 channels respectively. The outputs of the last convolution layer of IVIFNet are weight maps for infrared and visible images. Thus, the fusion result can be generated by using channel-wise multiplication with source images I_1, I_2 , which can be written as

$$I_f = \sum_{i=1}^2 \underbrace{C^4(F_n)}_{W_i} \otimes I_i, \quad (4)$$

where I_f denotes the fusion result. W_i is the i th weight map, which is calculated by conducting four convolutions on F_n . I_i represents i th source image.

C. Stage-interactive Feature Embedding Model

As shown in Fig. 3, vertically, our framework is consisted by multi-stage interactive feature embedding models (IFEMs). IFEMs conduct hierarchical feature interaction between SHFENet and IVIFNet. This allows to jointly learn correlative representations for alleviating vital feature missing in fusion result. We argue that the layers of SHFENet and IVIFNet can be treated as different feature descriptors, and features learned from different tasks can be treated as different representations of source images. Thus, feature representations related to reconstruction can provide additional vital features for fusion. Specifically, hierarchical feature interaction is conducted as a bridge between reconstruction and fusion task, which can utilize the internal relationship between different tasks to improve the feature representations, thereby boosting the performance of fusion task. The n -stage IFEM for hierarchical feature interaction between F_n and $F'_{n-1}, F''_{n-1}, F'_n, F''_n$ can be expressed as

$$F'_n, F''_n = Bi(F_n), F_n = INT(F'_{n-1}, F''_{n-1}), \quad (5)$$

where Bi denotes the hierarchical feature delivering process from IVIFNet to SHFENet, and INT represents the hierarchical feature delivering process from SHFENet to IVIFNet, which are equivalent to formulas (1) and (3), respectively. n denotes the stage number. Whereas the interaction process is bi-directional, F_n and F'_n, F''_n can be represented by each other.

To be specific, the INT process is designed to ensure that vital hierarchical features F'_n, F''_n are concatenated and shared to the corresponding hierarchical layer of fusion network, thereby promoting the fusion task. The stage-interactive INT process can greatly reduce the loss of intermediate information by leveraging all the hierarchical features for fusion. The Bi process aims to deliver the fused feature F_n to the reconstruction task, which in turn ensures that fused hierarchical feature F_n contains important information of source images. Therefore, stage-interactive feature embedding learning for hierarchical feature interaction between the reconstruction and fusion tasks can improve fusion performance.

D. Model Training

We aim to design a loss function to achieve vital feature extraction and fusion via interactive feature embedding in self-supervised learning framework. Specifically, we jointly train the reconstruction and fusion tasks. Thus, the designed loss can be expressed as

$$L = L_I + L_V + L_F + L_M, \quad (6)$$

where L_I and L_V are self-supervised reconstruction loss functions for SHFENet-ir and SHFENet-vis, respectively. L_F denotes the loss function for IVIFNet. L_M stands for weight map constraint.

Previous consistent loss functions (e.g., energy-based contrast constraint [37] and perceptual constraint [38]) generally fuse some specific information, such as luminance and edge. In contrast, we introduce a self-supervision constraint through designing a image reconstruction task, which is trained by regarding the source image as ground truth. Thus, more comprehensive features of source images can be learned. Here, we adopt the standard mean-square error (MSE) as loss function for self-supervised hierarchical feature extraction network training.

$$L_I = MSE(I_1, I_{r1}), L_V = MSE(I_2, I_{r2}), \quad (7)$$

where I_1 and I_2 represent the visible image and infrared image, I_{r1} and I_{r2} are the reconstructed results. The above loss functions ensure that hierarchical layers of reconstruction network own the ability of extracting vital features of the source images.

For further fusing the vital features, we adopt a loss function based on structural similarity index metric (SSIM) [39]–[41] for IVIFNet. Specifically, input images $I_n = I_n | n = 1, 2$ are represented by the components of contrast C , structure S and luminance l in SSIM framework:

$$I_n = C_n * S_n + l_n. \quad (8)$$

Contrast C_n and structure S_n are:

$$C_n = \|I_n - \mu_{I_n}\|, S_n = \frac{I_n - \mu_{I_n}}{\|I_n - \mu_{I_n}\|}, \quad (9)$$

where μ_{I_n} is the average value of I_n . For an expected result $\bar{I} = \xi \bar{C} * \bar{S}$, it should contain high contrast as well as the main structure of the source images. Thus, the corresponding contrast \bar{C} , structure \bar{S} can be expressed as

$$\bar{C} = \underbrace{\max}_{n=1,2} C_n, \bar{S} = \frac{\sum_{n=1}^2 S_n}{\|\sum_{n=1}^2 S_n\|}. \quad (10)$$

Finally, the SSIM between the fusion result I_f and the expected result \bar{I} can be calculated by the following function:

$$SSIM = \frac{2\sigma_{\bar{I}I_f} + C}{\sigma_{\bar{I}}^2 + \sigma_{I_f}^2 + C}, \quad (11)$$

where $\sigma_{\bar{I}}^2$ and $\sigma_{I_f}^2$ represent the variance of \bar{I} and I_f . $\sigma_{\bar{I}I_f}$ is the covariance of \bar{I} and I_f . Thus, the loss function for IVIFNet is calculated as

$$L_F = 1 - SSIM. \quad (12)$$

Weight map constraint L_M aims to adjust map values, thereby improving fusion performance. L_M can be written as

$$L_M = |\tau - W_1 - W_2|, \quad (13)$$

where τ is a hyperparameter.

IV. EXPERIMENTS

A. Implementation

The model is implemented with TensorFlow on GTX 2080TI GPU. Adam [42] optimizer with the learning rate of 1e-4 is adopted. The batch size is 1, and the momentum value

TABLE I

AVERAGE QUALITY METRICS OF DIFFERENT METHODS ON INFV-41 DATASET. THE BEST RESULT IS SHOWN IN **RED**, AND SECOND RESULT IS SHOWN IN **BLUE**.

	GTF	DTCWT	DeepFuse	DenseFuse	IFCNN	U2Fusion	FusionGAN	Ours
AG	4.888	7.154	6.153	6.161	8.752	7.458	3.662	10.18
EN	6.669	6.610	6.885	6.872	6.847	6.920	6.588	6.923
MI	13.34	13.22	13.77	13.75	13.69	13.84	13.18	13.85
GLD	8.562	12.49	10.85	10.85	15.28	13.17	6.638	17.96
SF	.0415	.0603	.0488	.0497	.0678	.0597	.0294	.0787
VIFF	.2205	.3834	.6080	.5988	.4774	.6955	.2923	.6414

TABLE II

AVERAGE QUALITY METRICS OF DIFFERENT METHODS ON INFV-20 DATASET. THE BEST RESULT IS SHOWN IN **RED**, AND SECOND RESULT IS SHOWN IN **BLUE**.

	GTF	DTCWT	DeepFuse	DenseFuse	IFCNN	U2Fusion	FusionGAN	Ours
AG	4.772	5.920	5.199	5.161	6.734	6.699	3.293	9.924
EN	6.611	6.414	6.732	6.899	6.638	6.783	6.449	6.787
MI	13.22	12.83	13.46	13.80	13.28	13.57	12.90	13.58
GLD	8.177	10.11	9.011	8.876	11.56	11.54	5.759	16.99
SF	.0398	.0490	.0397	.0431	.0526	.0505	.0266	.0770
VIFF	.1931	.3484	.6084	.4441	.4924	.6496	.2504	.7011

is 0.9. The weight decay is $5e-3$. τ and ξ are taken to 1.0 and 1.7, respectively. We train our model on the TNO database with 110 groups of infrared and visible images ¹.

B. Evaluation Criteria

We adopt six widely used objective metrics for evaluating the performance of our method and the competitors, e.g., Entropy (EN), Average gradient (AG), Gray level difference (GLD) [43], Mutual information (MI) [44], Spatial frequency (SF) [45] and visual information fidelity for fusion (VIFF) [46], which are consistent with subjective visual evaluation.

Average gradient (AG). AG reflects the clarity of fusion image, which represents the contrast of small details and local texture changes in the image. The larger AG, the more structure information retained in the fusion result.

$$AG = \frac{1}{(M-1)(N-1)} \sum_{i=1}^{M-1} \sum_{j=1}^{N-1} \sqrt{\frac{(I_f(i+1, j) - I_f(i, j))^2 + (I_f(i, j+1) - I_f(i, j))^2}{2}}, \quad (14)$$

where M and N are the width and height of fusion image I_f , and (i, j) denotes the location of each pixel.

Entropy (EN). Information theory-based EN denotes the average amount of information contained in an image, which is defined as:

$$En = - \sum_{i=1}^{L-1} p_i \log_2 p_i, \quad (15)$$

where L denotes the gray scale of image, p_i is the probability of gray value i appearing in the image. Larger En represents richer information in the image.

Mutual information (MI). MI can be used to measure the correlation between fused image and source images in the fusion field. Larger MI represents more vital information contained in the fusion result.

$$MI = MI(I_1, I_f) + MI(I_2, I_f), \quad (16)$$

where $MI(I_1, I_f)$ and $MI(I_2, I_f)$ denote the correlation among fusion result, infrared image, and visible image, respectively. $MI(I_n, I_f)$ is defined as:

$$MI(I_n, I_f) = E(I_n) + E(I_f) - E(I_n, I_f), \quad (17)$$

where $E(I_n)$ and $E(I_f)$ denote the information entropy of image I_n and I_f , respectively. $E(I_n, I_f)$ is the joint information entropy.

Gray level difference (GLD). GLD denotes the amount of the gradient information in the fused image. A larger GLD

¹https://figshare.com/articles/TN_Image_Fusion_Dataset/1008029.

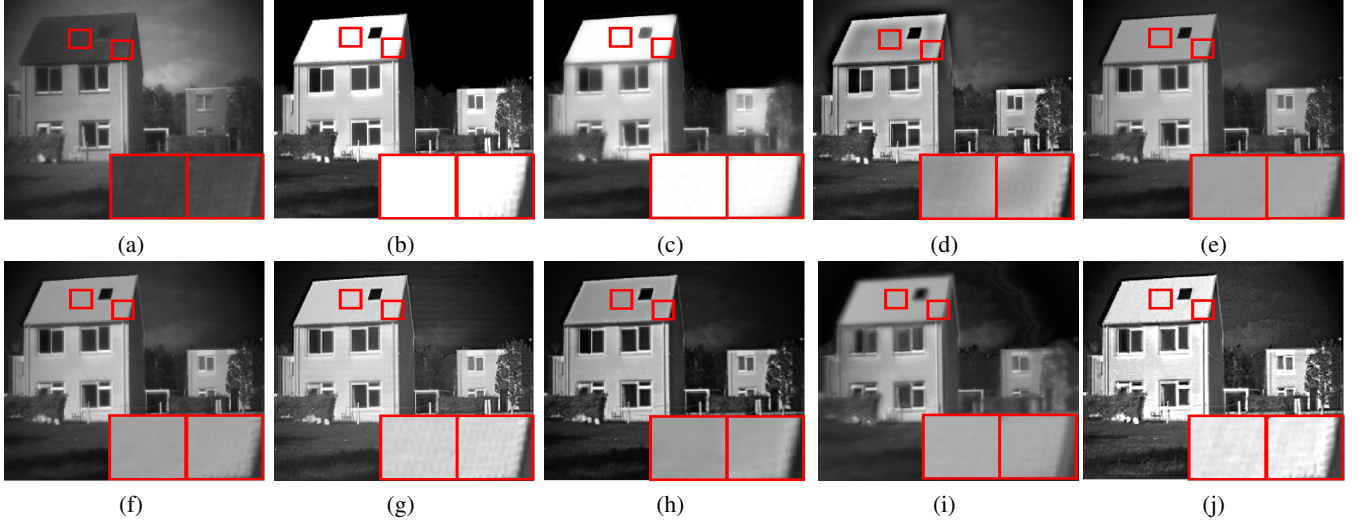


Fig. 4. Fusion result comparison of thermal radiation and visible texture information retention in infrared image and visible image, respectively. (a-j) correspond to the original visible and infrared images, and the fused results of GTF, DTCWT, DeepFuse, DenseFuse, IFCNN, U2Fusion, FusionGAN and our model.

stands for more texture information contained in the fused result.

$$GLD = \frac{1}{(M-1)(N-1)} \sum_{i=1}^{M-1} \sum_{j=1}^{N-1} | (I_f(i, j) - I_f(i+1, j)) | + | (I_f(i, j) - I_f(i, j+1)) |, \quad (18)$$

Spatial frequency (SF). SF reflects the change of image gray level, which is consisted by horizontal and vertical gradients. Larger SF denotes clearer fusion result.

$$SF = \sqrt{H^2 + V^2}, \quad (19)$$

where H and V are:

$$H = \sqrt{\frac{1}{MN} \sum_{i=1}^M \sum_{j=2}^N | I_f(i, j) - I_f(i, j-1) |^2}, \quad (20)$$

$$V = \sqrt{\frac{1}{MN} \sum_{i=2}^M \sum_{j=1}^N | I_f(i, j) - I_f(i-1, j) |^2}. \quad (21)$$

Visual information fidelity for fusion (VIFF). Since we aim to mitigate the vital information loss in the fused result, we adopt another evaluation matrix, named as VIFF [46]. VIFF measures the amount of visible information retained in the fused image, which is consistent with the human visual system. Thus, a larger VIFF represents that more visible information are fused into the fusion image, and less distortion between the fused result and source images.

C. Results and Analysis

In this section, we conduct qualitative and quantitative evaluations. The experiments are conducted on two widely used datasets for infrared and visible image fusion, named as INFV-20 dataset² and INFV-41 dataset³, respectively.

²https://github.com/hli1221/imagefusion_densefuse.

³<https://github.com/jiayi-ma/FusionGAN>.

For each dataset, we compare our model with seven state-of-the-art methods, including two hand-crafted feature-based methods, four non-adversarial CNN-based fusion methods, and one adversarial CNN-based fusion method, i.e., gradient transfer fusion (GTF) [26], DTCWT [47], DeepFuse [39], DenseFuse [11], IFCNN [12], U2Fusion [13], and FusionGAN [14].

1) *Quantitative Evaluation:* We firstly conduct quantitative comparison between our results and the results generated by the competitors using AG, EN, MI, GLD, SF and VIFF metrics on INFV-20 and INFV-41. Table I summarizes the average quality metrics of different methods on INFV-41 dataset. Obviously, our method achieves the best performance in terms of AG, EN, MI, GLD and SF metrics, and subprime performance on VIFF metric. The largest values of EN, AG, GLD and SF indicate that larger gradient, richer texture and higher contrast information are retained in the results. In addition, the satisfied values of MI and VIFF denote higher similarity between the result and source image, and meanwhile more visible information are retained in fusion image. Precisely, this proves the starting point of our approach that aims to fuse more vital information. Same conclusion can be drawn from Table II. Especially, DenseFuse and U2Fusion focus on extracting multi-level features contained in both visible and thermal images. Thus, they achieve better results of VIFF and MI, since the fused image retain the universal features of source images. In contrast, our fused image not only retains the universal features of source images, but also fuses discrepancy features of source images, thereby obtaining better results of AG, GLD and SF (where they comprehensively evaluate the performance of fused results, such as universal feature and discrepancy feature retention).

2) *Qualitative Evaluation:* We then conduct qualitative comparison with competitors. Visual comparisons on five pairs of representative images are provided in Figs. 4-7. In the subsection, we compare the retention of vital features of source images including both universal features and domain

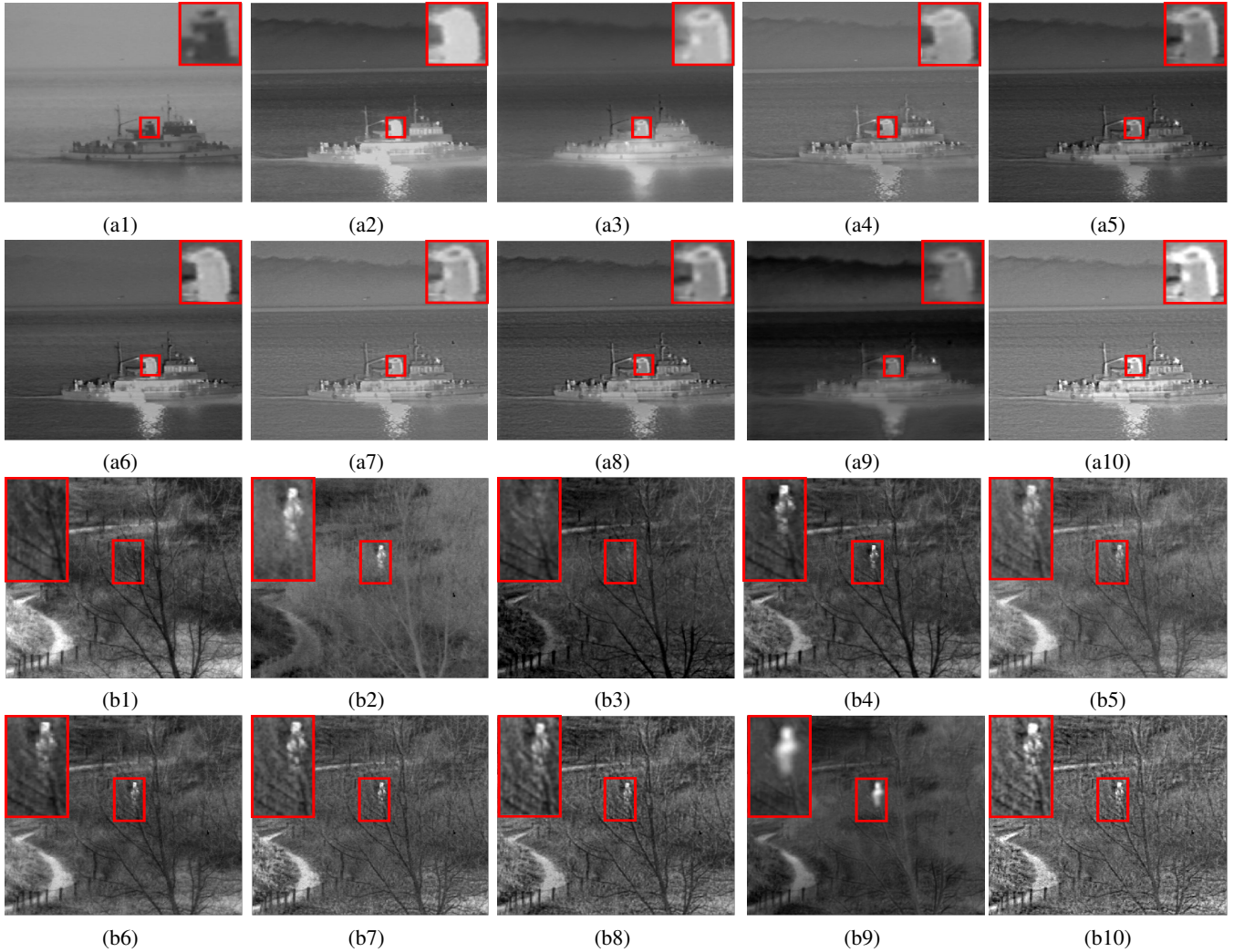


Fig. 5. Fusion result comparison of thermal radiation and visible texture information retention in infrared image and visible image, respectively. (a1-a10) and (b1-b10) correspond to the original visible and infrared images, and the fused results of GTF, DTCWT, DeepFuse, DenseFuse, IFCNN, U2Fusion, FusionGAN and our model.

discrepancy features.

Retaining of thermal radiation and texture information. As shown in Fig. 4(a) and Fig. 4(b), visible image is represented as gradient details while infrared image is mainly characterized as thermal radiation information. Thus, we evaluate the fusion performance from the perspective of the retention degree of such information.

As illustrated in Fig. 4, on the whole, all methods can fuse the main features of source images to some extent. More concretely, GTF can greatly fuse the thermal radiation information with high pixel intensity, while the structure features in visible image are lost. This can be explained that GTF aims to preserve the main intensity information of infrared image and gradient variation of visible image. As shown in the rectangular box of Fig. 4(c), the fusion result has strong intensity similarity with the infrared image, but the visible information (e.g., the roof of tile) is lost. As shown in the rectangular box of Fig. 4(d-e), both NSCT-SR and DTCWT cannot well retain the high intensity thermal information of infrared image, and loss partial of texture information of

visible image. Overall, those methods based on hand-crafted features can not well handle domain discrepancy between source images. Since low-level features cannot sufficiently represent thermal radiation information and visible appearance information, resulting in vital features missing.

Fig. 4(f-h) shows fusion results generated from non-adversarial based fusion methods. Intuitively, DeepFuse, DenseFuse and IFCNN cannot highlight the thermal information well, and partial gradient details of visible image are lost. We explain that those fusion methods focus on extracting and preserving vital features utilizing CNN structures via unsupervised strategy. On one hand, utilizing same convolution operator for generating weight maps or feature extraction, consequently leads to the loss of vital features which are specific to source images with domain discrepancy. On the other hand, the unsupervised training is achieved by optimizing loss function to constrain the fusion results containing the main contents of source images. Similarly, as shown in Fig. 4(i), FusionGAN based on adversarial training, also loses vital information, accompanied by ambiguity and distortion.

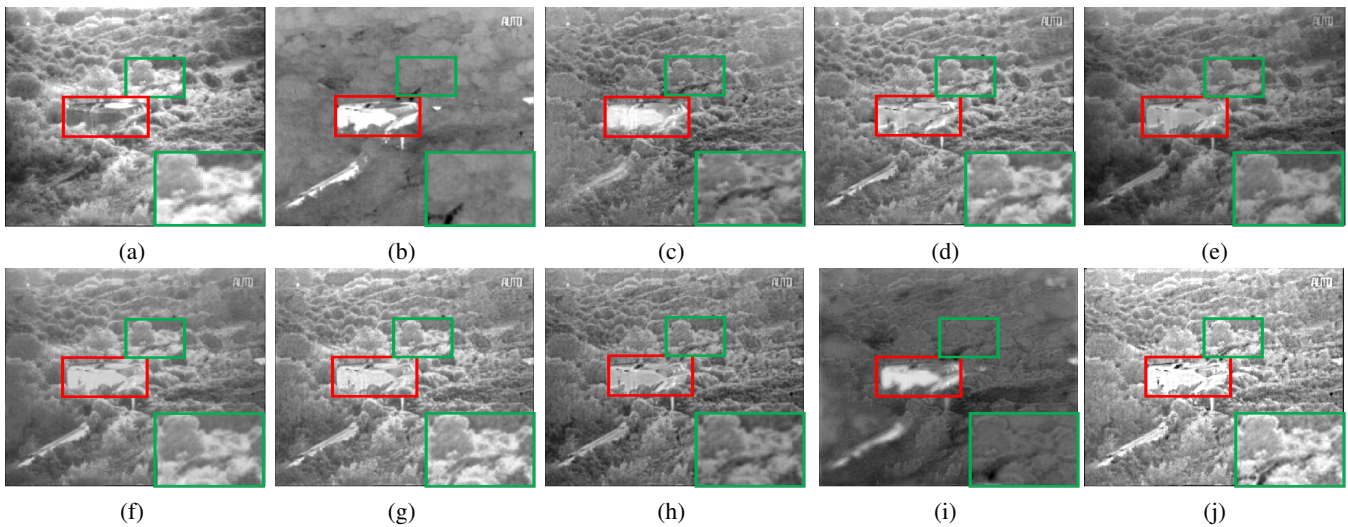


Fig. 6. Fusion result comparison of vital information retention in the visible image. (a-j) correspond to the original visible and infrared images, and the fused results of GTF, DTCWT, DeepFuse, DenseFuse, IFCNN, U2Fusion, FusionGAN and our model.

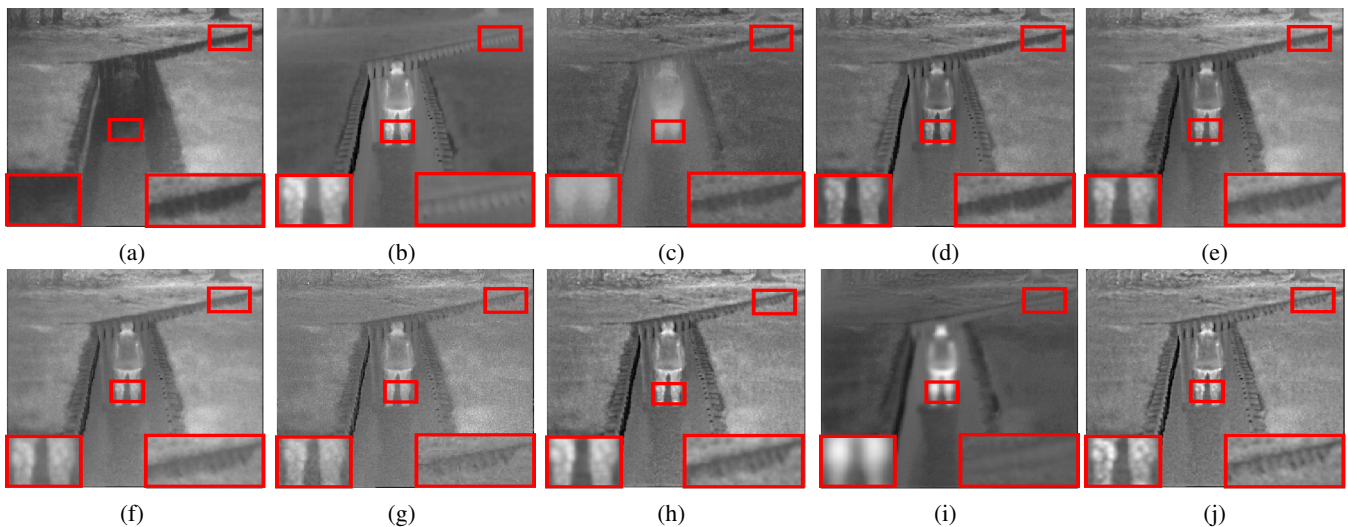


Fig. 7. Fusion result comparison of vital information retention in the infrared image. (a-j) correspond to the original visible and infrared images, and the fused results of GTF, DTCWT, DeepFuse, DenseFuse, IFCNN, U2Fusion, FusionGAN and our model.



Fig. 8. Fusion results by our method with the smooth constraint. Noise is suppressed in the fused images. The sources are in Fig. 1 and Figs. 4-7.

Thus, the unsupervised mechanism is unable to extract features adequately, which subsequently cannot guarantee all vital

information of source images can be retained. In contrast, as shown in Fig. 4(j), the vital information, including thermal information of infrared image and gradient details of visible image, are well retained in our fused result. Fig. 5 presents the fusion results on two representative image pairs. Obviously, our results also appear better fusion performance containing more vital information.

Retaining of other vital features. As discussed previously, not only thermal information with high pixel intensity is presented in infrared image, whereas, the other characteristics, such as gradient variation, texture and edge information are also included. In the same way, visible images also contain the other vital features, such as intensity, contrast and saturability. In this section, we further evaluate the retaining of other vital features of source images.

Fig. 6 presents the comparisons. It's worth noting that, here, we mainly focus on the retention of vital information in the visible image, in spite that our results can also maximum

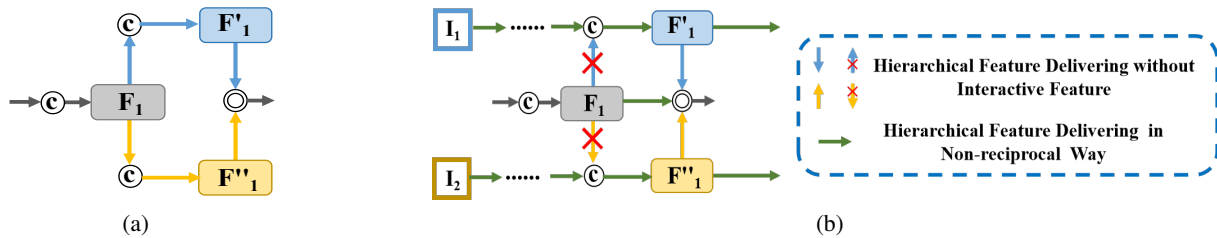


Fig. 9. (a) Basic constituent block (single stage IFEM) of IFESNet. (b) Basic constituent block of IFESNet w/o IFEM. IFESNet w/o IFEM adopts the same structure with IFESNet, but different feature stream. Instead of utilizing interactive feature between IVIFNet and SHFNet for gradually increasing extra vital information extraction, IFESNet w/o IFEM conducts hierarchical feature delivering in non-reciprocal way.

fusion of thermal radiation information in infrared images with higher contrast (as shown in the red rectangle box). More concretely, Fig. 6(a) presents abundant appearance, including high intensity, contrast and saturability information (as shown in the green rectangle box). As illustrated in Fig. 6(c), GTF can preserve the gradient variations of visible image, whereas the other vital information such as intensity, contrast and saturability is lost. The reason is that these features are not taken into account when modeling. The same issue appears in Fig. 6(d-e), which are generated by NSCT-SR and DTCWT, respectively. IFCNN can retain much more vital information from visible image compared with DeepFuse and DenseFuse. However, compared with visible image and our result, IFCNN still encounters certain degree of loss in brightness, contrast and saturation.

In addition, we further evaluate the retention of other vital features from infrared image, such as edge, gradient and texture information. A visual comparison is provided in Fig. 7. As shown in the highlighted regions of Fig. 7(b), the infrared image presents some texture information which is almost invisible in Fig. 7(a). Overall, as shown in the red boxes of Fig. 7(j), our result exhibits more texture appearance than the other methods. As illustrated in Fig. 7(c-i), the competitors lose some details, e.g., texture of legs, and edge of wall. This limits the application in scenario where gradient information is unavailable in visible image, whereas abundance in infrared image. Thus, our method can also preserve the detail information of infrared image more completely, which is ignored by other methods since they mainly focus on the thermal radiation information. Nevertheless, we attribute the excellent performance of our method to: 1) self-supervised strategy can generate more and comprehensive features of source image; 2) multi-stage interactive feature embedding learning can gradually integrate all vital information into fusion results and thus solve the vital information missing problem.

Discussion. Since image fusion focuses on generating a new image that retains source images' details, fused image will contain noise if the source image (e.g., infrared image) contains noise, as shown in Figs. 4-7. Here, we add a smooth constraint for the weight maps (see Eq. (4)) by using a Gaussian filter with variance 2 and window size 5×5 . The noise problem is relieved, as shown in Fig. 8. More denoising strategies (e.g., feature denoising) will be studied in future work.

TABLE III
EFFECT OF HIERARCHICAL FEATURE EXTRACTION VIA SELF-SUPERVISED STRATEGY ON INFV-41 DATASET.

	AG	EN	MI	GLD	SF	VIFF
IFESNet w/o IFEM	9.420	6.879	13.76	16.57	.0741	.5775
IFESNet	10.18	6.923	13.85	17.96	.0787	.6414

D. Ablation Study

Effect of Interactive Feature Embedding Learning. As described in Section III-B, interactive feature embedding model (IFEM) is designed, for promoting hierarchical feature extraction and fusion in the bi-directional interactive way. To analyze the contribution of this mechanism, we implement a variant named IFESNet w/o IFEM for comparison. The basic unit of IFESNet and IFESNet w/o IFEM are provided in Fig. 9(a) and Fig. 9(b). As shown in Fig. 9(b), the stage of IFESNet w/o IFEM is designed with the same architecture compared with Fig. 9(a), but the data flow direction is different. To be specific, instead of using interactive feature embedding learning mechanism between fusion and reconstruction tasks in IFESNet, IFESNet w/o IFEM only adopts hierarchical feature delivering from two reconstruction network without feature reverse delivering process from fusion network. Hence, hierarchical feature delivering is conducted in a non-reciprocal way. For a fair comparison, IFESNet and IFESNet w/o IFEM adopt identical convolution layers with the same parameters. Quantitative evaluations are shown in Table III and Table IV. Compared with IFESNet, IFESNet w/o IFEM results in poor fusion performance with all indexes decreased significantly. Although IFESNet w/o IFEM conducts hierarchical feature extraction in the self-supervised way, those hierarchical features without stage-interactive can't guarantee to contain vital information sufficiently for fusion.

Effect of Varied IFEM Stages. As shown in Fig. 9(a), we regard each layer of IFESNet and its corresponding layer of IVIFNet with one interactive feature embedding learning process, as a IFEM stage. In this study, we totally adopt three IFEM stages for vital feature extraction and fusion. In this section, we aim to analyze the performance of IFESNet with varied IFEM stages. To be specific, we compare IFESNet with one-stage (named as IFESNet-S1), two-stages (named as IFESNet-S2), three-stages (named as IFESNet-S3) and four-

TABLE IV
EFFECT OF HIERARCHICAL FEATURE EXTRACTION VIA SELF-SUPERVISED STRATEGY ON INFV-20 DATASET.

	AG	EN	MI	GLD	SF	VIFF
IFESNet w/o IFEM	9.102	6.719	13.44	15.53	.0720	.6161
IFESNet	9.924	6.809	13.62	16.99	.0770	.7011

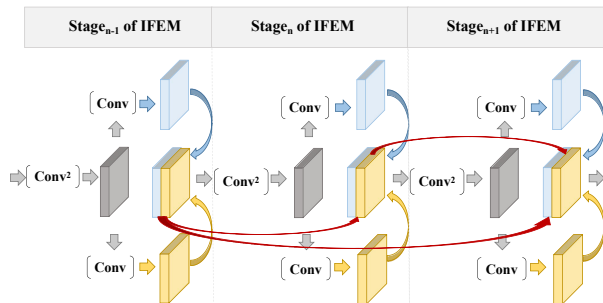


Fig. 10. Illustration of hierarchical connection of each stage. The feature generated by the $n - 1$ th stage is skipped (red arrows) to its later stage's features (e.g., the n th stage and the $n + 1$ th stage) by concatenation operation.

stages (named as IFESNet-S4). Quantitative evaluation of IFESNet and three variants on INFV-20 dataset and INFV-41 dataset are presented in Table V and Table VI, respectively.

As illustrated in Table V and Table VI, with the increase of stages, the evaluation criteria based on gradient information (e.g., AG, GLD and SF) tend to be smaller, while the evaluation criteria based on information entropy (e.g., EN), image similarity (e.g., MI) and fidelity (e.g., VIFF) tend to be larger. This can be explained as follows: when IFESNet adopts only a stage, the network itself pays more attention to the low-level features, such as texture and edge information. Thus the indexes based on gradient are higher. However, with the stage number increases, more high-level semantic information is extracted and then fused. In this case, the fusion appearance is closer to source image with more vital features while achieving better fidelity. Thus, by judging and weighing the fusion of both high-level and low-level features, three stages are adopted in the experiment.

As described above, with deepening of the network, more high-level semantic information is extracted and fused. Thus, the performance of the pixel-level fusion task may be limited. The hierarchical connection of each stage (denoted as IFESNet-HC) can deal with this dilemma, as shown in Fig. 10. The low-level and high-level features are integrated, thereby improving the fusion performance. In Table V, the hierarchical connection of each stage makes the deep network (four stages) achieve the best results.

Effect of self-supervised reconstruction loss. As described in Section III-D, we adopt MSE as loss function for self-supervised hierarchical feature extraction network training. Here, the MAE-based perceptual loss in the self-supervised mechanism is used for comparison. As shown in Table VI, our MSE-based loss can achieve better fusion performance.

Effect of structural similarity index loss. In order to

TABLE V
EFFECT OF VARIED BLOCKS FOR FUSION PERFORMANCE ON INFV-20 DATASET.

	AG	EN	MI	GLD	SF	VIFF
IFESNet-S1	10.20	6.758	13.52	17.52	.0796	.6705
IFESNet-S2	9.821	6.756	13.52	16.76	.0777	.6751
IFESNet-S3	9.924	6.809	13.62	16.99	.0770	.7011
IFESNet-S4	9.670	6.787	13.58	16.49	.0767	.7209
IFESNet-HC	11.10	6.817	13.64	18.94	.0860	.7566

TABLE VI
EFFECT OF SELF-SUPERVISED RECONSTRUCTION LOSS FOR FUSION PERFORMANCE ON INFV-20 DATASET.

	AG	EN	MI	GLD	SF	VIFF
MAE-based loss	9.762	6.773	13.55	16.77	.0765	.6997
MSE-based loss	9.924	6.809	13.62	16.99	.0770	.7011

retain source image's structural details, In Section III-D, we adopt structural similarity index metric (SSIM)-based loss to train IVIFNet. Here, the visible perception loss (VP) [37] is adopted for comparison. As shown in Table VII, our SSIM-based loss obtain better fusion performance, since the fused image preserves source image's structural details.

V. CONCLUSION

In this paper, a novel interactive feature embedding in self-supervised learning framework for infrared and visible image fusion is proposed for improving the vital information retention in fusion results. In particular, the self-supervised strategy is designed for capturing more informative representations of source images, which are adequately for jointly source image reconstruction and fusion. Moreover, stage-interactive feature embedding learning mechanism between a fusion network and two reconstruction networks is designed for embedding the vital information through stage-wise hierarchical feature interaction, which essentially is implemented by leveraging all the hierarchical features from different tasks. Qualitatively and quantitatively comparisons with the state of the arts indicate our method can not only better fuse the thermal radiation information of infrared image and the structural information of visible image, but also can retain the other vital information in infrared image (e.g., texture, edge) and visible image (e.g., intensity, contrast, saturation).

REFERENCES

- [1] X. Fan, P. Shi, J. Ni, and M. Li, "A thermal infrared and visible images fusion based approach for multitarget detection under complex environment," *Mathematical Problems in Engineering*, vol. 2015, no. PT.12, pp. 1774–1783, 2015. 1
- [2] R. Raghavendra, B. Dorizzi, A. Rao, and G. H. Kumar, "Particle swarm optimization based fusion of near infrared and visible images for improved face verification," *Pattern Recognition*, vol. 44, no. 2, pp. 401–411, 2011. 1

TABLE VII
EFFECT OF STRUCTURAL SIMILARITY INDEX LOSS FOR FUSION
PERFORMANCE ON INFV-20 DATASET.

	AG	EN	MI	GLD	SF	VIFF
VP-based loss	8.417	6.451	12.90	14.12	.0639	.2425
SSIM-based loss	9.924	6.809	13.62	16.99	.0770	.7011

- [3] I. Ulusoy and H. Yuruk, "New method for the fusion of complementary information from infrared and visible images for object detection," *Iet Image Processing*, vol. 5, no. 1, pp. 36–0, 2011. 1
- [4] Y. Wang, Y. Xiao, J. Lu, B. Tan, Z. Cao, Z. Zhang, and J. T. Zhou, "Discriminative multi-view dynamic image fusion for cross-view 3-d action recognition," *IEEE Transactions on Neural Networks and Learning Systems*, pp. 1–14, 2021. 1
- [5] J. Chen, X. Li, L. Luo, X. Mei, and J. Ma, "Infrared and visible image fusion based on target-enhanced multiscale transform decomposition," *Information Sciences*, vol. 508, 08 2019. 1, 2
- [6] S. Li, B. Yang, and J. Hu, "Performance comparison of different multi-resolution transforms for image fusion," *Information Fusion*, vol. 12, no. 2, pp. 74–84, 2011. 1, 2
- [7] X. Jin, Q. Jiang, S. Yao, D. Zhou, R. Nie, S.-J. Lee, and K. He, "Infrared and visible image fusion method based on discrete cosine transform and local spatial frequency in discrete stationary wavelet transform domain," *Infrared Physics and Technology*, vol. 88, pp. 1 – 12, 2018. 1, 2
- [8] Y. Liu, S. Liu, and Z. Wang, "A general framework for image fusion based on multi-scale transform and sparse representation," *Information Fusion*, vol. 24, pp. 147–164, 2015. 1, 2
- [9] Z. Zhou, B. Wang, S. Li, and M. Dong, "Perceptual fusion of infrared and visible images through a hybrid multi-scale decomposition with gaussian and bilateral filters," *Information Fusion*, vol. 30, 11 2015. 1, 2
- [10] M. Yin, P. Duan, W. Liu, and X. Liang, "A novel infrared and visible image fusion algorithm based on shift-invariant dual-tree complex shearlet transform and sparse representation," *Neurocomputing*, vol. 226, 11 2016. 1, 2
- [11] H. Li, "Densefuse: A fusion approach to infrared and visible images," *IEEE Transactions on Image Processing*, vol. 28, pp. 2614–2623, 12 2018. 1, 2, 7
- [12] Y. Zhang, Y. Liu, P. Sun, H. Yan, X. Zhao, and L. Zhang, "Ifcnn: A general image fusion framework based on convolutional neural network," *Information Fusion*, vol. 54, pp. 99–118, 2020. 1, 7
- [13] H. Xu, J. Ma, J. Jiang, X. Guo, and H. Ling, "U2fusion: A unified unsupervised image fusion network," *IEEE Transactions on Pattern Analysis and Machine Intelligence*, pp. 1–1, 2020. 1, 2, 7
- [14] J. Ma, W. Yu, P. Liang, C. Li, and J. Jiang, "Fusiongan: A generative adversarial network for infrared and visible image fusion," *Information Fusion*, vol. 48, pp. 11–26, 08 2019. 1, 3, 7
- [15] J. Ma, H. Xu, J. Jiang, X. Mei, and X.-P. Zhang, "Ddrgan: A dual-discriminator conditional generative adversarial network for multi-resolution image fusion," *IEEE Transactions on Image Processing*, vol. PP, pp. 1–1, 03 2020. 1, 3
- [16] J. Ma, P. Liang, W. Yu, C. Chen, X. Guo, J. Wu, and J. Jiang, "Infrared and visible image fusion via detail preserving adversarial learning," *Information Fusion*, vol. 54, pp. 85–98, 2020. 1, 3
- [17] Q. Zhang and M. D. Levine, "Robust multi-focus image fusion using multi-task sparse representation and spatial context," *IEEE Transactions on Image Processing*, vol. 25, no. 5, pp. 2045–2058, 2016. 2
- [18] J. Wang, J. Peng, X. Feng, G. He, and J. Fan, "Fusion method for infrared and visible images by using non-negative sparse representation," *Infrared Physics and Technology*, vol. 67, pp. 477–489, 2014. 2
- [19] J. Ma, Y. Ma, and C. Li, "Infrared and visible image fusion methods and applications: A survey," *Information Fusion*, vol. 45, pp. 153–178, 01 2019. 2
- [20] Q. Zhang, Y. Liu, R. S. Blum, J. Han, and D. Tao, "Sparse representation based multi-sensor image fusion for multi-focus and multi-modality images: A review," *Information Fusion*, vol. 40, pp. 57–75, 2018. 2
- [21] X. Lu, B. Zhang, Y. Zhao, H. Liu, and H. Pei, "The infrared and visible image fusion algorithm based on target separation and sparse representation," *Infrared Physics and Technology*, vol. 67, pp. 397–407, 11 2014. 2
- [22] Z. Wang, X. Jin, N. Zhou, and Y. Zhao, "Infrared and visible images fusion based on rpca and nsct," *Infrared Physics and Technology*, vol. 77, pp. 114–123, 2016. 2
- [23] N. Mitianoudis and T. Stathaki, "Pixel-based and region-based image fusion schemes using ica bases," *Information Fusion*, vol. 8, pp. 131–142, 04 2007. 2
- [24] W. Kong, Y. Lei, and H. Zhao, "Adaptive fusion method of visible light and infrared images based on non-subsampled shearlet transform and fast non-negative matrix factorization," *Infrared Physics and Technology*, vol. 67, pp. 161–172, 2014. 2
- [25] W. Zhao, Z. Xu, and J. Zhao, "Gradient entropy metric and p-laplace diffusion constraint-based algorithm for noisy multispectral image fusion," *Information Fusion*, vol. 27, pp. 138–149, 2016. 2
- [26] J. Ma, C. Chen, C. Li, and J. Huang, "Infrared and visible image fusion via gradient transfer and total variation minimization," *Information Fusion*, vol. 31, pp. 100–109, 2016. 2, 7
- [27] F. Zhao, W. Zhao, L. Yao, and Y. Liu, "Self-supervised feature adaption for infrared and visible image fusion," *Information Fusion*, vol. 76, pp. 189–203, 2021. 2
- [28] R. Dian, S. Li, and X. Kang, "Regularizing hyperspectral and multi-spectral image fusion by cnn denoiser," *IEEE Transactions on Neural Networks and Learning Systems*, vol. 32, no. 3, pp. 1124–1135, 2021. 2
- [29] Y. Liu, X. Chen, J. Cheng, H. Peng, and Z. Wang, "Infrared and visible image fusion with convolutional neural networks," *International Journal of Wavelets, Multiresolution and Information Processing*, vol. 16, 12 2017. 2
- [30] H. Li, X. J. Wu, and J. Kittler, "Infrared and visible image fusion using a deep learning framework," in *International Conference on Pattern Recognition 2018*, 2018. 2
- [31] W. Zhao, D. Wang, and H. Lu, "Multi-focus image fusion with a natural enhancement via a joint multi-level deeply supervised convolutional neural network," *IEEE Transactions on Circuits and Systems for Video Technology*, vol. 29, no. 4, pp. 1102–1115, 2018. 2
- [32] H. Zhang, H. Xu, Y. Xiao, X. Guo, and J. Ma, "Rethinking the image fusion: A fast unified image fusion network based on proportional maintenance of gradient and intensity," *Proceedings of the AAAI Conference on Artificial Intelligence*, vol. 34, pp. 12797–12804, 04 2020. 2
- [33] R. Dian, S. Li, A. Guo, and L. Fang, "Deep hyperspectral image sharpening," *IEEE Transactions on Neural Networks and Learning Systems*, vol. 29, no. 11, pp. 5345–5355, 2018. 2
- [34] X. Fu, W. Wang, Y. Huang, X. Ding, and J. Paisley, "Deep multiscale detail networks for multiband spectral image sharpening," *IEEE Transactions on Neural Networks and Learning Systems*, vol. 32, no. 5, pp. 2090–2104, 2021. 2
- [35] F. Zhao, W. Zhao, H. Lu, Y. Liu, L. Yao, and Y. Liu, "Depth-distilled multi-focus image fusion," *IEEE Transactions on Multimedia*, 2021. 2
- [36] Y. Gao, J. Ma, M. Zhao, W. Liu, and A. L. Yuille, "Nddr-cnn: Layerwise feature fusing in multi-task cnns by neural discriminative dimensionality reduction," in *Proceedings of the IEEE/CVF conference on computer vision and pattern recognition*, 2019, pp. 3205–3214. 4
- [37] F. Zhao and W. Zhao, "Learning specific and general realm feature representations for image fusion," *IEEE Transactions on Multimedia*, vol. 23, pp. 2745–2756, 2020. 5, 11
- [38] B. Lu, J.-C. Chen, and R. Chellappa, "Unsupervised domain-specific deblurring via disentangled representations," in *Proceedings of the IEEE Conference on Computer Vision and Pattern Recognition*, 2019, pp. 10225–10234. 5
- [39] K. Ram Prabhakar, V. Sai Srikar, and R. Venkatesh Babu, "Deepfuse: A deep unsupervised approach for exposure fusion with extreme exposure image pairs," in *Proceedings of the IEEE International Conference on Computer Vision (ICCV)*, 10 2017, pp. 4724–4732. 5, 7
- [40] K. Ma, H. Li, H. Yong, Z. Wang, D. Meng, and L. Zhang, "Robust multi-exposure image fusion: A structural patch decomposition approach," *IEEE Transactions on Image Processing*, vol. 26, no. 5, pp. 2519–2532, 2017. 5
- [41] H. Li, K. Ma, H. Yong, and L. Zhang, "Fast multi-scale structural patch decomposition for multi-exposure image fusion," *IEEE Transactions on Image Processing*, vol. PP, no. 99, pp. 1–1, 2020. 5
- [42] D. P. Kingma and J. Ba, "Adam: A method for stochastic optimization," *arXiv preprint arXiv:1412.6980*, 2014. 5
- [43] W. Zhao, H. Lu, and D. Wang, "Multisensor image fusion and enhancement in spectral total variation domain," *IEEE Transactions on Multimedia*, vol. 20, no. 4, pp. 866–879, 2017. 6
- [44] R. Nava, G. Cristóbal, and B. Escalante-Ramrez, "Mutual information improves image fusion quality assessments," *SPIE News Room*, vol. 34, pp. 94–109, 2007. 6

- [45] Y. Zheng, E. A. Essock, B. C. Hansen, and A. M. Haun, "A new metric based on extended spatial frequency and its application to dwt based fusion algorithms," *Information Fusion*, vol. 8, no. 2, pp. 177–192, 2007. [6](#)
- [46] Y. Han, Y. Cai, Y. Cao, and X. Xu, "A new image fusion performance metric based on visual information fidelity," *Information Fusion*, vol. 14, no. 2, pp. 127 – 135, 2013. [6](#), [7](#)
- [47] S. Li, B. Yang, and J. Hu, "Performance comparison of different multi-resolution transforms for image fusion," *Information Fusion*, vol. 12, no. 2, pp. 74–84, 2011. [7](#)